ACS OMEGA

Open Access

http://pubs.acs.org/journal/acsodf

Article

A Novel Approach for Comprehensive Utilization by Leaching Pyrite Cinder with Titanium Dioxide Waste Acid by Response Surface Methodology

Congxue Tian*

Cite This: *ACS Omega* 2024, 9, 8510−8519

Read Online

ACCESS | Metrics & More | Article Recommendations

ABSTRACT: Comprehensive utilization of two industrial wastes by leaching pyrite cinder with titanium dioxide waste acid was proposed by using response surface methodology of the Box−Behnken design method. The effects of leaching conditions such as leaching temperature, leaching time, and waste acid/pyrite cinder ratio on the leaching yield were examined. The prediction model including the leaching variables with a good fitting result was established to predict the leaching yield or optimize the leaching variable values. The regression equation model was significant and reliable with an actual correlation coefficient R^2 of 0.9856. The leaching conditions greatly affected the leaching rate, reaction equilibrium, solubility of the acid decomposed substances, and the common ion effects, influenced the leaching process, and finally improved the leaching yield. The variables such as leaching temperature and waste acid/pyrite cinder ratio had the greatest collaborative interactions, and the effects of the waste acid/pyrite cinder ratio were larger than the other two. The verification experiments confirmed that the leaching yield values could be achieved at 82.68 % under the optimal conditions.

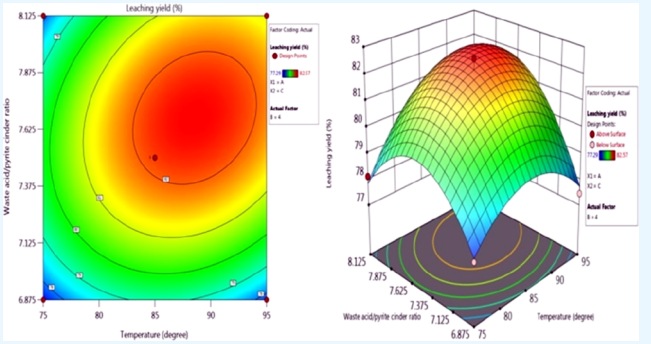

1. INTRODUCTION

With the rapid development of industry, the pollution and harm of industrial byproducts to the environment are becoming increasingly serious. China was a major producer of sulfuric acid, ranking the third place in the world.[1] The production of sulfuric acid through pyrite roasting was one of the main sources of sulfuric acid in China, accounting for about 16.9 %, and for every 1 ton of sulfuric acid produced, approximately 0.8−1.1 tons of pyrite cinder would be produced.[2] In 2022, 9504.6×10^4 tons of sulfuric acid was produced in China, resulting in approximately 1700×10^4 tons of pyrite cinder byproducts. The pyrite cinder referred to the waste residue discharged during the production of sulfuric acid using pyrite as raw material and was an industrial tailing. Due to the fact that pyrite cinder was fired from natural minerals, its composition was complex and varies greatly. The main components of the cinder were unreacted raw materials and byproducts.[3] The main components were the phases such as hematite (Fe_2O_3), magnetite (Fe_3O_4), and some phases containing silicon, magnesium, aluminum oxides, etc. The most important and abundant element in the cinder was iron. Due to the different origins and sources of the pyrite, the iron content fluctuated greatly, usually ranging from 40% to 60%. A large amount of waste residues was disposed by landfill or directly stacked, which not only wasted resources and occupied a large amount of land but also caused varying degrees of pollution to the soil, water, and atmospheric environment.[4,5] With the depletion of mineral resources and the widespread utilization of iron ore, the comprehensive utilization of sulfuric acid slag has become an urgent problem that needs to be solved. At present, the comprehensive utilization of pyrite cinder mainly included preparation of iron salts, iron-based pigments, iron oxides, polymeric ferric sulfate, and water purification flocculants using pyrite cinder as the raw material.[6−10] In recent years, pyrite cinder had also been used to prepare confined photo-Fenton catalytic materials through simple leaching adsorption calcination methods and applied in removal of reactive azo dye from aqueous solutions.[11,12] And these methods provided new ideas for comprehensive utilization of pyrite cinder.

The titanium resources reserved in China ranked first in the world, with 870 million tons of vanadium titanium magnetite resources in the Pan-Xi region alone, accounting for 35% of global titanium resources. Due to its mineral structure and high calcium and magnesium content, it was mainly used to produce

Received: December 8, 2023
Revised: January 25, 2024
Accepted: January 29, 2024
Published: February 7, 2024

titanium dioxide by the sulfate process.[13] The main source of titanium dioxide waste acid was the filtrate formed during the filtration of metatitanic acid with a sulfuric acid content of about 20%. The second source was dilute acidic water generated during the washing of metatitanic acid, with a sulfuric acid content of about 5%. In the sulfate process for TiO_2 production, for every 1 ton of TiO_2 pigment produced, approximately 6−8 tons of waste sulfuric acid with a concentration of about 20% would be produced as a byproduct.[14] The treatment of titanium dioxide waste acid mainly included two methods: neutralization and comprehensive recovery; most of the waste acid was directly neutralized with lime to form titanium gypsum for storage. Approximately 3.364 million tons of titanium dioxide pigments were produced by using the sulfate process in China in 2022, resulting in about 27 million tons of 20% waste sulfuric acid, which would cause great harm to the environment. In recent years, a series of studies had been conducted on valuable metal extraction, harmless resource utilization, recovery of titanium and sulfuric acid, and pressure leaching of titanium concentrate,[15−19] providing useful references for the comprehensive utilization of TiO_2 pigment waste acid.

The response surface methodology (RSM) could be used to investigate the significance of the effects of model equations, optimize process conditions, predict response values under certain conditions, and evaluate the impact of various process conditions on experimental results. RSM could also investigate interactive effects between process conditions, compensating for the limitations of a single factor influence in ordinary orthogonal optimization experiments. RSM was used to optimize enzymatic hydrolysis conditions of shrimp in order to improve product addedvalue and reduce environmental pollution for the shrimp aquaculture industry.[20] The optimization method for leaching process conditions of difficult to select flotation copper tailings adopts RSM, and the variation patterns of influencing factors and the optimal leaching conditions were obtained.[21] The RSM using central composite design (CCD) was used to study the effects of leaching time, liquid−solid ratio, and ammonia concentration on zinc mixed leaching, and the optimized leaching conditions were obtained.[22] The leaching process of copper in low-grade flotation was optimized using RSM under key conditions of sulfuric acid concentration, nitric acid concentration, and leaching time, and the leaching conditions and leaching rate were correlated to obtain a quadratic model equation.[23] The process of leaching copper from the old AMD Athlon processor was optimized by using response surface methodology and central composite rotatable design (CCRD) with nitric acid concentration, temperature, and ultrasound power as influencing variables.[24] Using RSM to conduct statistical experimental designs was an efficient approach to implement experimental research, and in which the Box−Behnken design (BBD) was a more effective approach to optimize the processing after limiting the parameters' range and could obtain the best results with a small number of experiments.[25]

If ferrous sulfate could be prepared by leaching pyrite cinder from titanium dioxide waste acid and using it as an iron source for lithium iron phosphate battery material production, achieving the recovery of Fe, S and the comprehensive utilization of the two industrial waste byproducts, and realizing Ti−Fe−S coproduction new process and low-cost manufacturing of ferrous sulfate, it would provide new research ideas and application directions for the comprehensive utilization of waste byproducts.

2. EXPERIMENTAL SECTION

The pyrite cinder obtained from the sulfuric acid production process by using pyrite concentrate as raw material was leached by titanium dioxide waste acid. The composition of pyrite cinder was dry based total Fe of 61.08%, FeO of 17.22%, Fe_2O_3 of 68.22%, and a moisture content of 10.74% (wt). The composition of titanium dioxide waste acid was the ferrous ion concentration of 58.58 g/L, sulfuric acid mass concentration of 20.58%, and density of 1.335 g/mL. The leaching reaction was conducted in a four port round-bottom flask with heating, stirring, and condensation reflux. The leaching conditions such as leaching temperature, leaching time, and waste acid/pyrite cinder ratio had important impacts on the leaching yield of pyrite cinder leached by titanium dioxide waste acid. Taking into account the factors such as the rate and efficiency of the leaching reaction, heating energy consumption, and the solubility of iron sulfate and ferrous sulfate, the following leaching conditions had been selected. And the typical leaching process operation was as follows: weighed 80 g of pyrite cinder and placed it into the reactor, and then a certain amount of titanium dioxide waste acid (550 g, 600 g, and 650 g) was added to the reactor to maintain a certain waste acid/pyrite cinder ratio. Under mechanical stirring at 300 rpm, the pyrite cinder and waste acid were mixed evenly, and then the reacting system was gradually heated to a certain temperature (75 °C, 85 °C, 95 °C) for the leaching experiment and maintained unchanged. The leaching reaction ended after a certain time (3 h, 4 h, and 5 h). Added 200 mL of boiling water to the leached slurry, then performed vacuum filtration, and washed with 300 *mL* of boiling water. Diluted the obtained filtrate with cold water to 1210 g to avoid crystallization and precipitation of ferrous sulfate after cooling and measured the diluted filtrate's density after cooling to room temperature.

The total iron content of the dried pyrite cinder and diluted leaching filtrate was determined according to the standard GB/T 6730.5−2007 *Iron ores-determination of total iron content-titanium*(III) chloride reduction methods. The iron (II) content of the dried pyrite cinder and diluted leaching filtrate was determined according to the standard GB/T 6730.8-2016 *Iron ores-determination of iron(II) content-potassium dichromate titrimetric method*. And the iron (III) content was equal to the total iron content minus the iron (II) content. The leaching yield could be calculated by the following formula: (where TFe means total iron)

$$\text{Leaching Yield} = \frac{\text{TFe(leachingfiltrate)} - \text{TFe(wasteacid)}}{\text{TFe(pyritecinder)}} \times 100\%$$

The crystal structure of the unleached and leached pyrite cinder was determined by an X-ray powder diffractometer (X' Pert3 Powder, PANalytical). The morphologies and element composition distribution scanning of the samples were observed by scanning electron microscopy (Zeiss EVO 18, Germany) with an energy dispersive spectrometer (EDS, XFlash 6130, Bruker, Germany).

3. RESULTS AND DISCUSSIONS

To explore the effects of leaching parameters on the leaching yield for pyrite cinder, the three main factors (leaching temperature (X_1), leaching time (X_2), and waste acid/pyrite cinder ratio (X_3)) were selected to construct the experimental design as function variables. The *BBD* experiments of the RSM method was used to optimize the leaching conditions for

https://doi.org/10.1021/acsomega.3c09815
ACS Omega 2024, 9, 8510−8519

Table 1. Factors and Levels of BBD Experiments for Leaching Conditions

factors	−1	0	1
leaching temperature (°C), X_1	75	85	95
leaching time (h), X_2	3	4	5
waste acid/pyrite cinder ratio, X_3	6.875	7.500	8.125

Table 2. Experimental Design Matrix, Experimental Leaching Yield Results, and Predicted Ones

no.	X_1 (°C)	X_2 (h)	X_3	Y measured (%)	Y predicted (%)
1	75	4	6.875	77.34	77.47
2	75	5	7.500	78.20	78.21
3	85	5	8.125	79.30	79.56
4	75	4	8.125	78.12	77.85
5	95	5	7.500	81.36	81.22
6	75	3	7.500	78.67	78.81
7	95	3	7.500	79.28	79.27
8	85	3	6.875	77.29	77.03
9	85	3	8.125	79.69	79.83
10	95	4	8.125	81.19	81.06
11	85	4	7.500	81.86	82.16
12	85	4	7.500	82.05	82.16
13	85	5	6.875	78.79	78.65
14	95	4	6.875	77.45	77.73
15	85	4	7.500	82.57	82.16

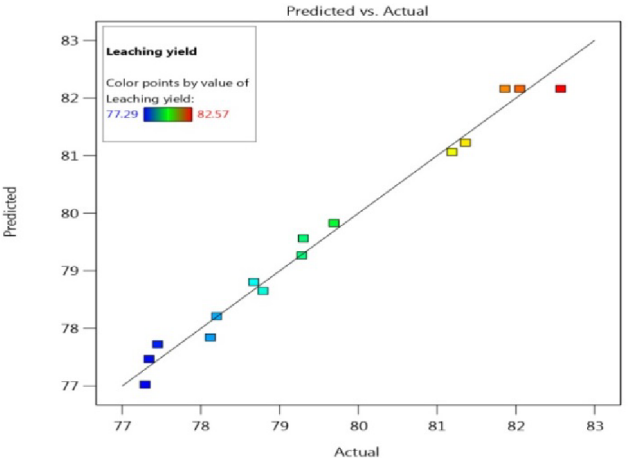

Figure 2. Actual leaching yield values plotted against the predicted values derived from the model.

extracting pyrite cinder from TiO_2 waste acid, a total of 15 experiments were conducted to ensure experimental accuracy and the impact of experimental errors on variance analysis. Taking leaching yield (Y) as the response value and the three leaching parameters that significantly influenced the leaching yield were treated as the investigation factors, the BBD test factors and levels are shown in Table 1. All experimental runs

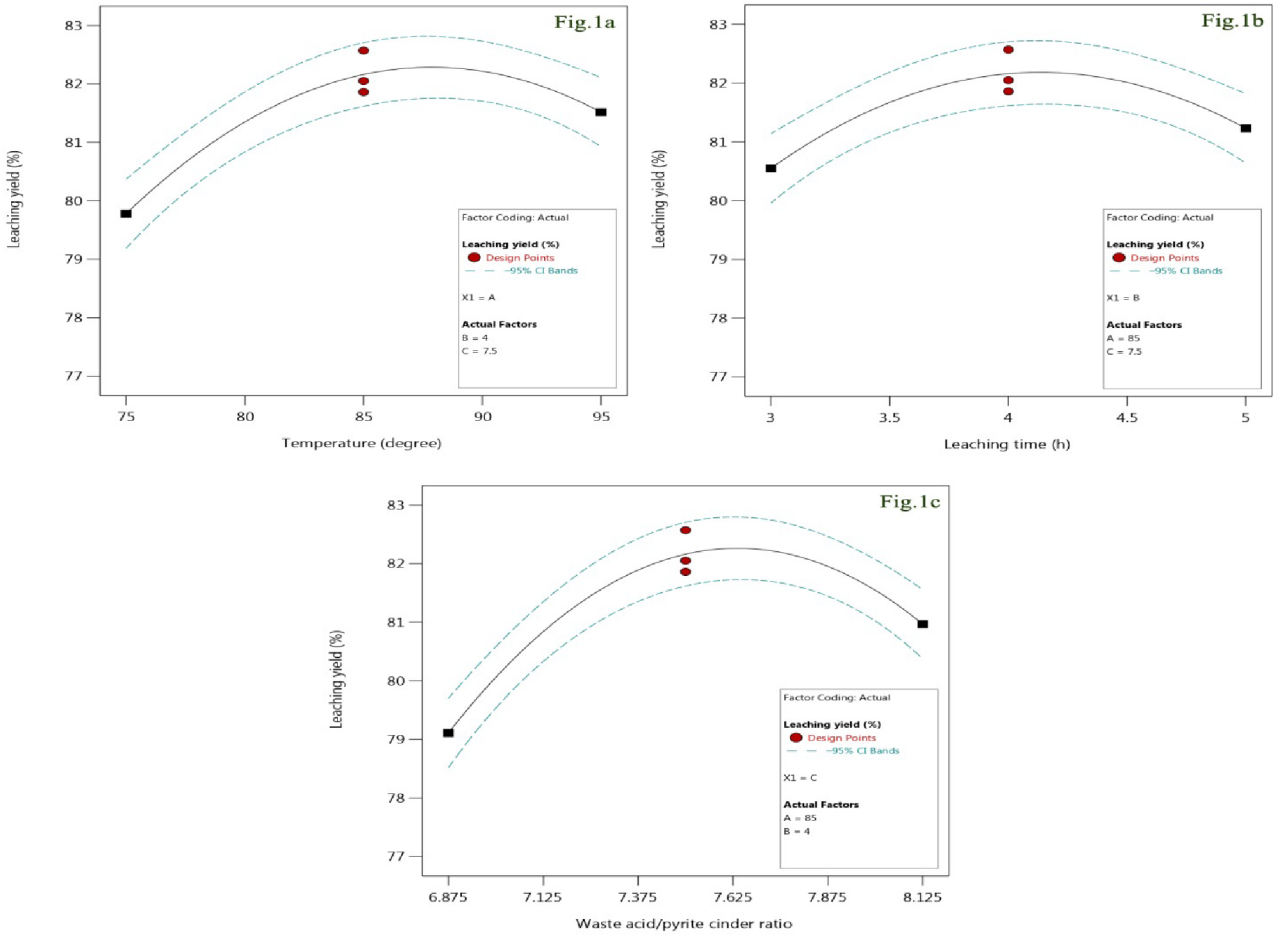

Figure 1. Effects of leaching conditions on the leaching yield (a) leaching time at 4 h, waste acid/pyrite cinder ratio at 7.5; (b) leaching temperature at 85 °C, waste acid/pyrite cinder ratio at 7.5; and (c) leaching temperature at 85 °C, leaching time at 4 h.

https://doi.org/10.1021/acsomega.3c09815
ACS Omega 2024, 9, 8510−8519

Table 3. Variance Analysis of Response Surface Experiments Results for the Leaching Yield[a]

source	sum of squares	df	mean square	*F*-value	*p*-value	significant
model	45.778785	9	5.086531667	38.01735242	0.000447223	**
X_1	6.0378125	1	6.0378125	45.12734033	0.001107264	**
X_2	0.9248	1	0.9248	6.912066968	0.046584829	*
X_3	6.9006125	1	6.9006125	51.57601181	0.000814606	**
X_1X_2	1.625625	1	1.625625	12.15011772	0.017551101	*
X_1X_3	2.1904	1	2.1904	16.37131432	0.009862745	**
X_2X_3	0.893025	1	0.893025	6.674576778	0.049221663	*
X_1^2	8.446730769	1	8.446730769	63.13188661	0.000508937	**
X_2^2	5.955323077	1	5.955323077	44.51080442	0.001142609	**
X_3^2	16.63386923	1	16.63386923	124.3235489	0.000101205	**
residual	0.668975	5	0.133795			
lack of fit	0.398775	3	0.132925	0.983900814	0.539767744	
pure error	0.2702	2	0.1351			
cor total	46.44776	14				
R^2				0.9856		
R^2_{Adj} = 0.9597, R^2_{Pred} = 0.8495						
C.V.%				0.4598		

[a]"*" indicated that it had a significant impact on the results ($p < 0.05$), "**" indicated that it had a very significant impact on the results ($p < 0.01$).

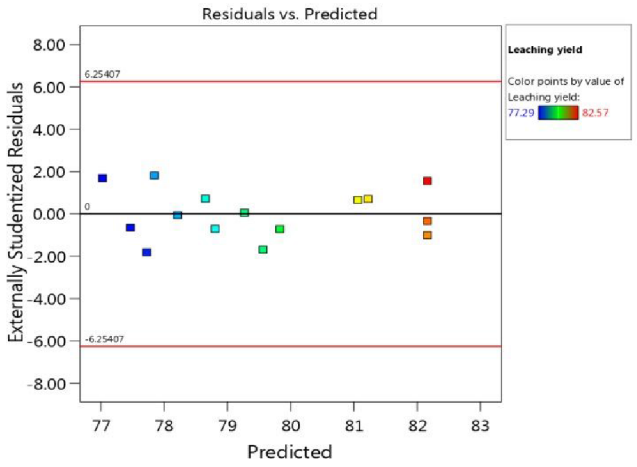

Figure 3. Residuals vs predicted derived from the model.

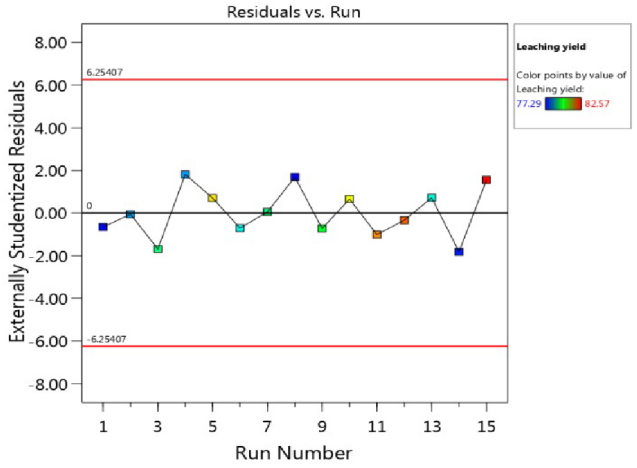

Figure 4. Residuals vs run derived from the model.

were consistent with Table 2, and the test actual leaching yield values and predicted ones are shown in Table 2.

When fixing the leaching time at 4 h and waste acid/pyrite cinder ratio at 7.5, with the increasingleaching temperature, the

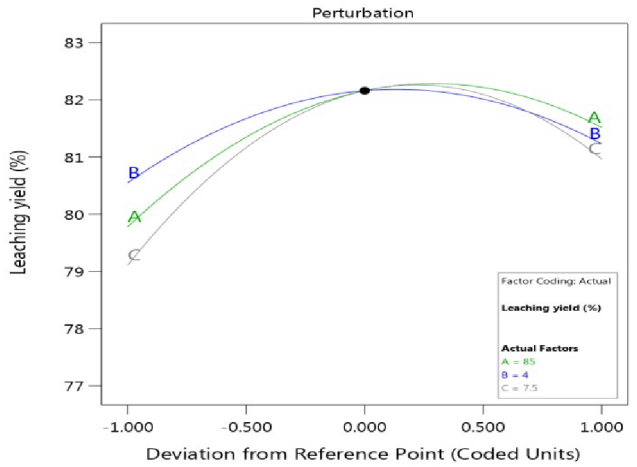

Figure 5. Perturbation plot for the leaching yield.

leaching yield for the pyrite cinder first increased and then decreased, as shown in Figure 1a. The leaching temperature mainly affected leaching rate, leaching reaction equilibrium, and solubility of the acid decomposed substances. With the increase in the leaching temperature, the reaction velocity would accelerate, which would shorten the completion time for the leaching reaction to reach the reacting equilibrium. The leaching reaction slowed as the temperature increased, mainly because the leaching reaction released heat, thereby affecting the leaching equilibrium. As the leaching reaction proceeded, the concentration of $Fe_2(SO_4)_3$ in the solution increased. Due to the interaction between $Fe_2(SO_4)_3$ molecules, the dissolution process was hindered, resulting in a decrease in the solubility of the main component $Fe_2(SO_4)_3$, which in turn led to a decrease in leaching yield. These combined effects of these influencing factors showed that there was an appropriate leaching reaction temperature in the range 85°C−95 °C in the leaching system.

When fixing the leaching temperature at 85°C and waste acid/pyrite cinder ratio at 7.5, the leaching yield was first increased and then decreased with the increasing leaching time, as shown in Figure 1b. As the leaching time was prolonged, the

https://doi.org/10.1021/acsomega.3c09815
ACS Omega 2024, 9, 8510−8519

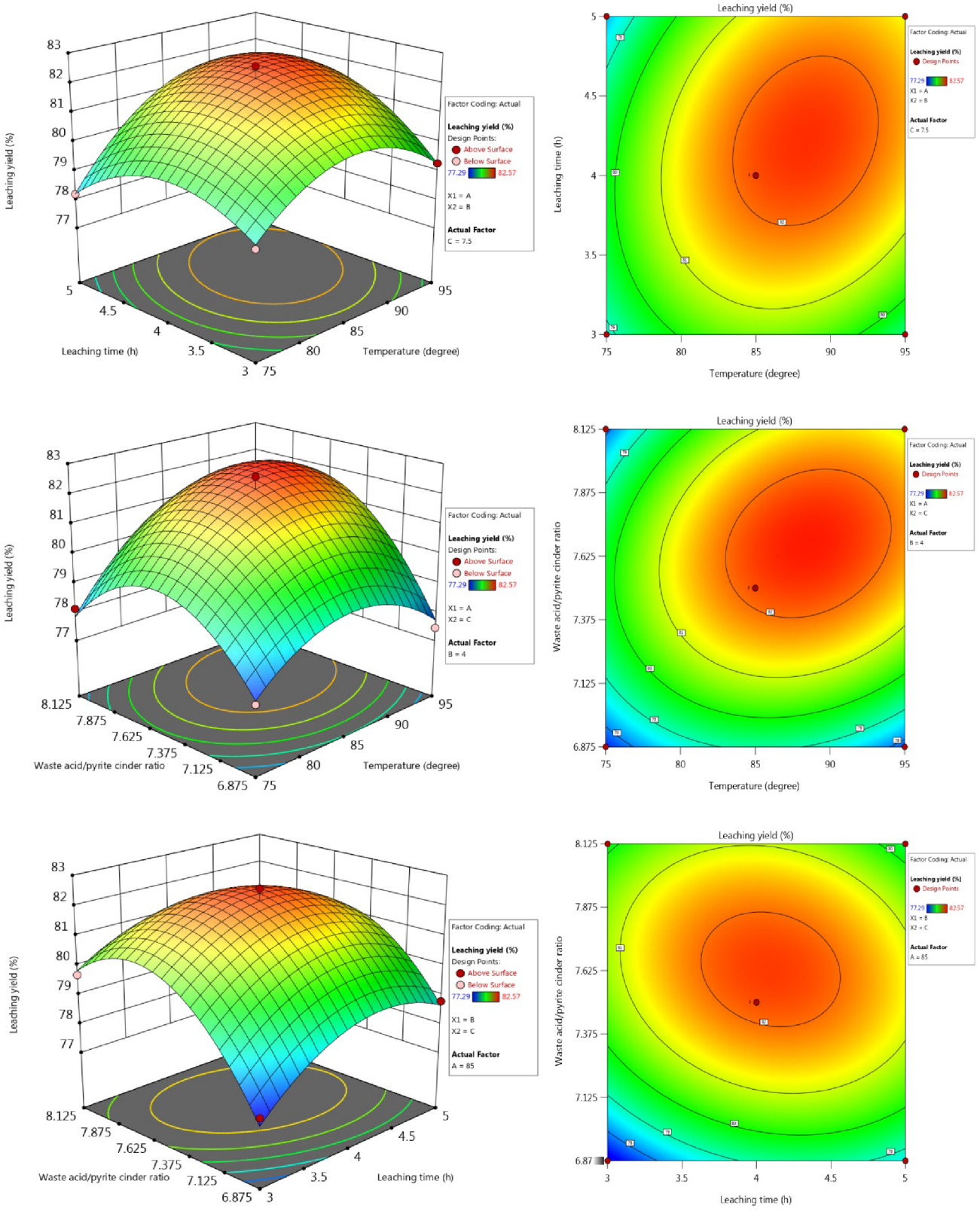

Figure 6. Response surface plots and contour lines of interaction factors on the leaching yield.

concentration of leaching products such as $Fe_2(SO_4)_3$ in the solution gradually increased. Some solutes were reduced in solubility due to changing system properties and were induced to precipitate by the small particles in the suspension system, resulting in a decrease in the measured iron content and a decrease in the leaching yield. An appropriate leaching time was beneficial for avoiding the precipitation of the aforementioned solutes, thereby improving the leaching yield of the pyrite cinder.

When fixing the leaching temperature at 85°C and leaching time at 4 h, with the waste acid/pyrite cinder ratio increasing, the

https://doi.org/10.1021/acsomega.3c09815
ACS Omega 2024, 9, 8510−8519

Table 4. Results of Verification Tests

no.	leaching temperature (°C)	leaching time (h)	waste acid/pyrite cinder ratio	leaching yield (%)
optimized	88.904	4.183	7.667	82.485
16	89	4.18	7.67	82.68
17	89	4.18	7.67	82.83
18	89	4.18	7.67	82.53

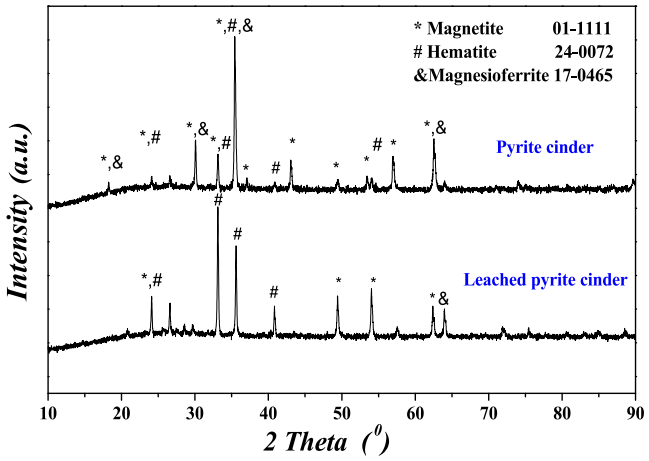

Figure 7. XRD patterns for the pyrite cinder samples.

leaching yield first increased and then decreased, as shown in Figure 1c. With the increase of waste acid dosage, the amount of acid in the leaching system increased, promoting the reaction progress and reaction equilibrium to move forward and improving the leaching yield. When the acid content was too high, due to the introduction of more sulfate ions in the leaching system, the same ion effect led to a decrease in the solubility of the leaching product such as $Fe_2(SO_4)_3$ and $FeSO_4$, resulting in a decrease in the leaching yield. The waste acid/pyrite cinder ratio had the greatest impact on the leaching yield, indicating that the effects of the waste acid/pyrite cinder ratio had a greater impact than the other two parameters.

From the leaching yield results for the pyrite cinder (Y) (Table 2), the model equation between the leaching yield and the leaching conditions (X_1, X_2, X_3) is obtained as follows:

$$Y = 82.16 + 0.8687X_1 + 0.3400X_2 + 0.9287X_3 + 0.6375X_1X_2 + 0.7400X_1X_3 - 0.4725X_2X_3 - 1.51X_1^2 - 1.27_2^2 - 2.12X_3^2 \quad (1)$$

Each absolute coefficient value in directly reflected the impacts of the factor on the leaching yield value, and the positive and negative values of the coefficients indicated the direction of their impact. It could be seen that the influence order was $X_3 > X_1 > X_2$, that was, waste acid/pyrite cinder ratio > leaching temperature> leaching time.

The empirical relationship could also be written as the following equation represented by actual values. This could not only predict the corresponding leaching yield of pyrite cinder based on the equation resulting from the values of the leaching factors but also optimize the corresponding values of the factors by presetting the leaching yield value.

$$Y = -298.49250 + 1.51512X_1 + 10.75125X_2 + 75.95000X_3 + 0.063750X_1X_2 + 0.118400X_1X_3 - 0.756000X_2X_3 - 0.015125X_1^2 - 1.27000X_2^2 - 5.43360X_3^2 \quad (2)$$

The actual leaching yield values and the predicted values were listed in Figure 2 and Table 2, and the predicted ones were very close to the experimental values. The predicted values highly matched the actual data with $R^2 = 0.9856$, as shown in Table 3, implying that 98.56% of the predicted values fell within the range of experimental leaching yield variation. The predicted Y value range was slightly narrower than the actual value range, mainly due to experimental deviations during the leaching process as well as the errors in iron content determination, ultimately leading to this phenomenon. However, its relative error was within 0.5%, which was acceptable. From the adjusted correlation coefficient ($R^2_{adj} = 0.9597$) for the leaching yield of pyrite cinder, which was very close to the correlation coefficient R^2, it could be seen that the regression of the predicted leaching yield value was very close to the actual data because the predicted R^2 with the value of 0.8495 and the adjusted R^2 with the value of 0.9597 were relatively consistent and reasonable, which also proved that the regression equation model was significant and reliable. From the residual versus predicted plot (Figure 3), each data point showed a random distribution pattern at both ends of the Y-axis at 0, and there were no obvious identifiable patterns in the points, indicating that the residual distribution was random and relatively constant. When displayed in sequence, the residuals vs run plots (Figure 4) were randomly distributed around the centerline, without showing trends or patterns, which could verify the hypothesis that residuals were independent of other residuals. The perturbation plot (Figure 5) indicated that the influence of A, B, and C factors on leaching yield showed a curve effect, and as the level of factors increased, the leaching yield showed a trend of first rapid increase and then slow decrease. From the variation amplitude and steepness of the three-factor perturbation plot for the leaching yield (Figure 5), it could be seen that the influence of the leaching yield was greatest for factor C, followed by factor A, and the smallest for factor B, which was consistent with the previous variance analysis results (Table 3).

The main and collaborative interaction effects of these leaching conditions on the leaching yield of pyrite cinder were determined by variance analysis (Table 3). The F-value (38.02) indicated that the regression model was very significant, with only a 0.04% chance of such a large F-value occurring due to noise, indicating that the effects of leaching conditions were very significant. As the p-value (0.0004) of the regression model was much smaller than 0.01, it indicated that the significance level of the model was very high. The main leaching parameters X_1, X_2, and X_3 had very significant effects on the leaching yield results ($p < 0.05$), and the collaborative interaction items X_1X_2, X_1X_3, and X_2X_3 had also significant effects on the leaching yield results ($p < 0.05$). All the influences of quadratic terms X_1^2, X_2^2, and X_3^2 on the leaching results were also very significant as for $p < 0.01$. Because R^2 was very close to 1, the predicted values of the regression equation were highly consistent with the experimental values, showing a high correlation. And the $C.V.$ value was of 0.4598%, which was very low, indicating that the experimental values were reliable. This also confirmed that using

https://doi.org/10.1021/acsomega.3c09815
ACS Omega 2024, 9, 8510−8519

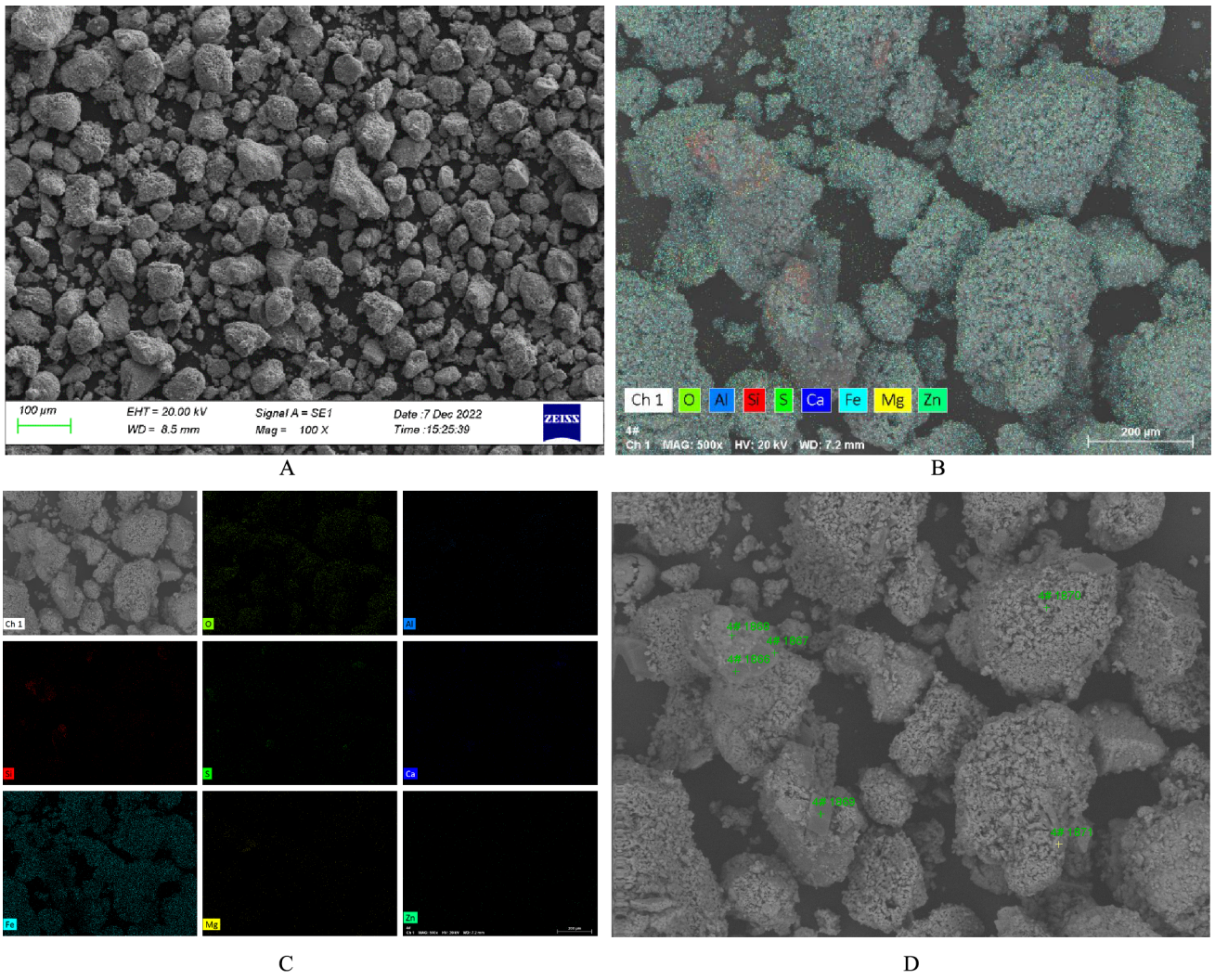

Figure 8. SEM photographs and EDS analysis for the raw pyrite cinder. (A) SEM photograph for the pyrite cinder; (B) surface scanning photograph; (C) surface scanning results of various elements; (D) point scanning positions of various elements.

Table 5. EDS Analysis of Element Content for the Pyrite Cinder

	element content (wt %)									
point number	O	Na	Mg	Al	Si	S	K	Ca	Mn	Fe
4# 1866	31.80	0.80	13.89	9.54	19.17	1.03	3.22	0.96	1.99	17.05
4# 1867	31.97	0.78	9.17	6.14	17.83	1.04	1.30		0.87	30.91
4# 1868	8.77		1.60	1.32	3.09	0.31	0.52			84.38
4# 1869	26.37					25.52		37.64		10.48
4# 1870	24.11	0.51		0.75	1.62	0.42	0.29	0.97		71.32
4# 1871	6.15				1.55			1.15		91.15

the response surface method of the Box−Behnken design could achieve good regression and realize model prediction.

The response surface 3D diagram and contour in Figure 6 could intuitively reflect the collaborative interactions of the leaching parameters on the leaching yield and the values of various parameters under optimal conditions. All the response surface 3D diagrams of the interaction between two factors were steep, indicating that they had a significant impact on the leaching yield. And all the 3D diagrams were raised shapes, indicating that there were maximum leaching yield values for the pyrite cinder. All the closed ellipse of contour lines indicated that there were significant collaborative interactions between leaching temperature, leaching time, and waste acid/pyrite cinder ratio, which was consistent with the variance analysis results in Table 3. When the leaching temperature was 85 °C, the leaching time was 4 h, the waste acid/pyrite cinder ratio was 7.5, and the leaching yield value could reach the experimental maximum value of 82.57 %.

By stepwise regression the equation, the optimum leaching conditions for the predicted maximum leaching yield value (82.485%) were determined as follows: the leaching temperature was of 88.904 °C, leaching time was of 4.183 h, and waste acid/pyrite cinder ratio was of 7.667. To facilitate the control of leaching conditions, the leaching temperature of the validation experiment was adjusted to 89 °C, the leaching time was adjusted to 4.18 h, and the waste acid/pyrite cinder ratio was

https://doi.org/10.1021/acsomega.3c09815
ACS Omega 2024, 9, 8510−8519

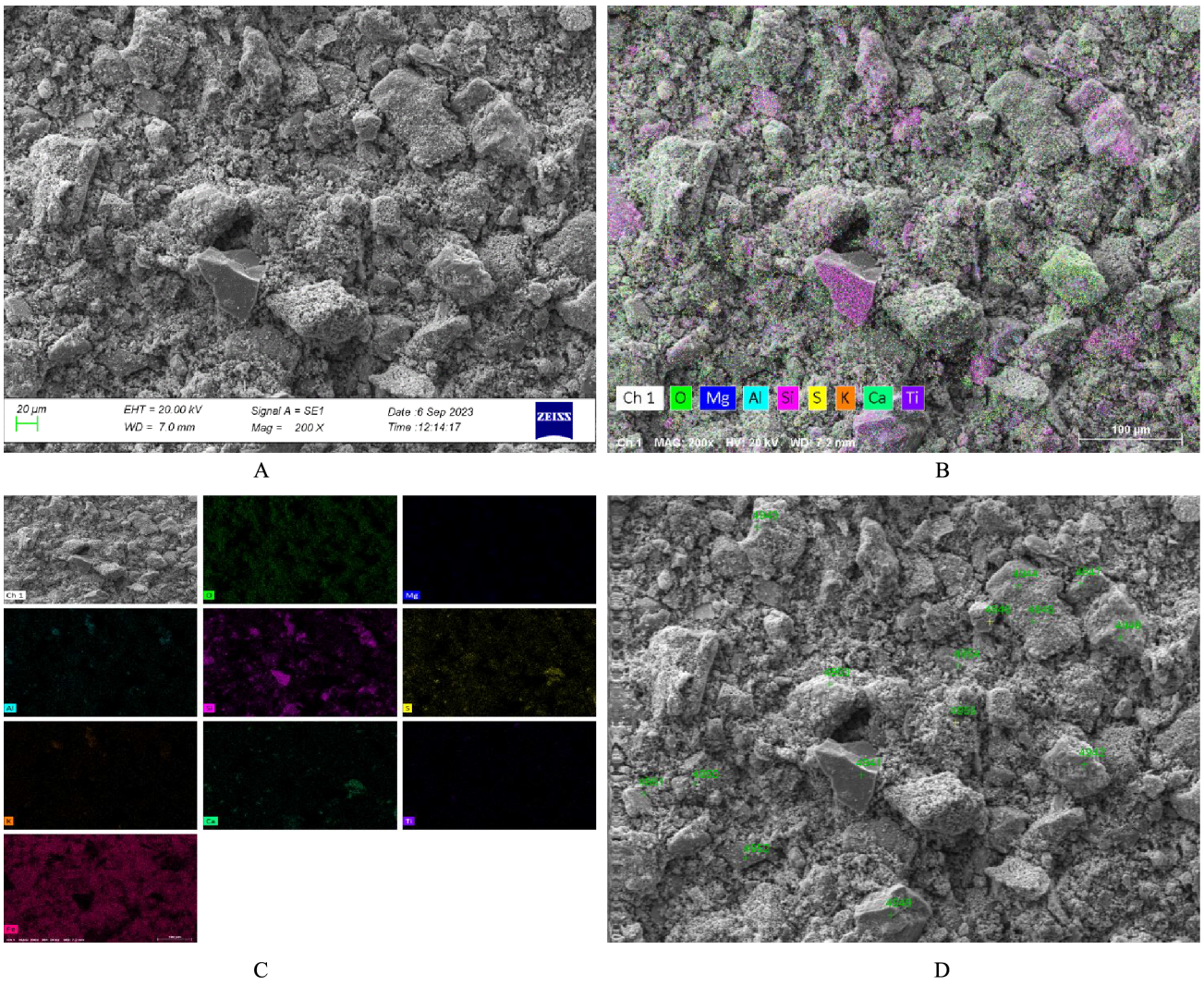

Figure 9. SEM photographs and EDS analysis for the leached pyrite cinder; (A) SEM photograph for the leached pyrite cinder; (B) surface scanning photograph; (C) surface scanning results of various elements; (D) point scanning positions of various elements.

Table 6. EDS Analysis of Element Content for the Leached Pyrite Cinder

	element content (wt %)										
point number	O	Na	Mg	Al	Si	S	K	Ca	Mn	Ti	Fe
4941	27.15				68.58						4.26
4942	46.36					19.91		29.59			4.13
4943	24.44					0.86					74.71
4944	5.59				1.52	0.85					92.05
4945	25.39				1.82	2.17					70.61
4946	3.35				1,29						95.36
4947	35.72		0.97	1.67	14.00	5.20	0.97			17.16	24.31
4948	39.24				57.88						2.89
4949	23.90	1.58	8.54		30.35			11.73			23.90
4950	9.89				1.63	3.98		1.88			82.62
4951	3.58			0.93	3.26	2.54					89.68
4952	10.46										89.54
4953	11.74			1.16	16.62	7.26		0.81			62.41
4954	16.09				0.48	0.65					56.87
4955	1.81		0.84	1.46	2.63	1.61					91.66

adjusted to 7.67. The verification test results for leaching yield were listed in Table 4, and the average leaching yield was 82.68%. The relative average standard deviation for the verification test results was only 0.15%, and the relative average standard deviation for the verification test and predicted value was only 0.18%. The high consistency with the predicted values

https://doi.org/10.1021/acsomega.3c09815
ACS Omega 2024, 9, 8510−8519

of the model indicated a good fit between the predicted values and the experimental values, further verifying the reliability of the regression model.

The XRD patterns of the unleached and leached pyrite cinder are shown in Figure 7. The XRD pattern of the uneached pyrite cinder showed that its phases were mainly composed of Fe_3O_4, Fe_2O_3, and Mg_2SiO_4, with the former two phases as the main components. Due to the fact that sulfuric acid production from pyrite concentrate was carried out at 700°C−900 °C, the generated iron containing phases such as Fe_3O_4 and Fe_2O_3 were relatively stable and had strong reaction inertness, resulting in relatively difficult leaching of the pyrite cinder under dilute acid conditions. Even after enhanced leaching, there were still some unreacted phases in the leaching residue, such as Fe_3O_4 and Fe_2O_3, which further confirmed the claim that these phases were somewhat inert. Optimizing and regulating the leaching conditions would help to improve the leaching yield for pyrite cinder.

The SEM photographs and EDS analysis for the pyrite cinder are showed in Figure 8 and listed in Table 5. The particles of pyrite cinder exhibited irregular shapes and varying sizes in Figure 8A, with particle sizes ranging from 20 μm to 150 μm, mainly concentrated in the range of 40−70μm. In Figure 8B, from the magnified backscattered electron image, it could be seen that large particles of the pyrite cinder were formed by the aggregation of small particles, which would form many pores and facilitate the entry, diffusion, and reaction of sulfuric acid during the acid leaching reaction. The element surface distribution diagram of the pyrite cinder sample under 20 kV accelerated voltage is shown Figure 8C, indicating that Fe and O were mainly present in the sample, in addition to a large amount of Si and a small amount of Al, S, Ca, Mg, and Zn. The EDS results of scanning 6 points in the backscattered electron image (Figure 8D) are listed in Table 5. The selected points all contained Fe and O, especially the three points numbered 4 # 1868, 4 # 1870, and 4 # 1871, which mainly existed in the form of iron oxides. And all the selected point scan results showed the presence of various impurity elements. The EDS results showed that in addition to iron oxides, there were also oxidized substances such as Si, Al, S, Ca, Mg, Zn, Na, K, and Mn distributed in the pyrite cinder.

The SEM photographs and EDS analysis for the leached pyrite cinder are shown in Figure 9 and listed in Table 6. After acid leaching, most of the iron-containing phases, calcium, magnesium, and aluminum containing phases, and other phases decomposed and entered into the liquid phase. The particles became significantly smaller and powdery, much smaller than unleached samples, as shown in Figure 9A. However, there were some large particle phases containing silicon that had not reacted with dilute sulfuric acid, and there were also small amounts of iron-containing substances that had not been fully acidulated in the phases, as shown in Figure 9B,C. And the particle size of the coarse particles was in the range of 20−90 μm. The element surface distribution diagram of the leached sample is shown in Figure 9, indicating that elements of O, Si, Fe, and S were mainly present in the sample, except for a small amount of Mg, Al, K, Ca, and Ti. The EDS results of the selected scanning points in the backscattered electron image (Figure 9) are listed in Table 6. The composition of low iron content sites was mainly composed of silicon and calcium oxide, while the higher iron content sites were high iron containing substances such as Fe_2O_3 and Fe_3O_4 that had not been completely decomposed, as mentioned above. Substances containing silicon and calcium were prone to forming silicates and calcium sulfate during the leaching reaction, which then precipitated and coated the surface of the unreacted particles, hindering further reaction and leading to a decrease in the leaching yield of the pyrite cinder. If these products could be further peeled off from the surface of the reaction particles, it would help to improve the leaching yield.

4. CONCLUSIONS

The comprehensive utilization of two industrial wastes containing iron and sulfur resources had been achieved by leaching pyrite cinder with titanium dioxide waste acid. Using response surface methodology of the Box−Behnken design method, the effects of leaching conditions such as leaching temperature, leaching time, and waste acid/pyrite cinder ratio were investigated on the leaching yield of pyrite cinder. The leaching rate, reaction equilibrium, solubility of the acid decomposed substances, and the common ion effects were significantly influenced by the leaching conditions, and appropriate leaching conditions would help to improve the leaching yield of the pyrite cinder. Through BBD experimental design, suitable regression equations were established, and variance analysis was conducted. The correlation coefficient(R^2 = 98.56%) of the regression model was very high, which proved the applicability of this method in determining and optimizing the leaching conditions for the pyrite cinder. The actual value of leaching yields is highly consistent with the predicted values, which verified the adequacy and effectiveness of the prediction model. The obtained regression equation reached a significant level, also proving the reliability of the experimental operation. The leaching variables had obvious collaborative interactions, and the effect of the waste acid/pyrite cinder ratio on the leaching yield was larger than the other two parameters. The insoluble substances formed by Si and Ca wrapped around the pyrite cinder, which was the key reason hindering further leaching of the pyrite cinder. It was necessary to consider removing them as the key to further improving the leaching yield. Under the optimal leaching conditions, the verification experimental results also proved that the leaching yield could reach the corresponding predicted values, which further confirmed the reliability of the regression model. These results indicated that the optimization by using RSM based on the BBD approach was an effective method to obtain the optimal leaching conditions for leaching pyrite cinder from TiO_2 waste acid with a high yield.

■ ASSOCIATED CONTENT

Data Availability Statement

All data generated or analyzed during this study are included in this manuscript.

■ AUTHOR INFORMATION

Corresponding Author

Congxue Tian − *Panzhihua University, Panzhihua, Sichuan 617000, PR China;* orcid.org/0000-0001-8482-0169; Email: tcx7311@163.com

Complete contact information is available at: https://pubs.acs.org/10.1021/acsomega.3c09815

Author Contributions

The author (C.T.) obtained all the funding, proposed the relevant concepts and methods, designed experiments, con-

https://doi.org/10.1021/acsomega.3c09815
ACS Omega 2024, 9, 8510−8519

ducted experimental research, and wrote and revised the manuscript.

Notes

The author declares no competing financial interest.

■ ACKNOWLEDGMENTS

This study was supported by Major Scientific and Technological Research Project of Panzhihua Xichang Strategic Resource Development (CCJ [2022] No. 390-1-9), Science and Technology Achievement Transfer and Transformation Guidance Plan of Sichuan Province (23ZHSF0237), Sichuan Provincial Science and Technology Plan Transfer Payment Special Project (22ZYZF-GG-02 and 22ZYZF-GG-05), and Science and Technology Service Industry Project of Sichuan Province (2022KJFWYSF-1, Xingzhong Titanium Industry).

■ REFERENCES

(1) Zhang, J. F.; Yan, Y.; Hu, Z. H.; Fan, X. Z.; Zheng, Y. Utilization of low-grade pyrite cinder for synthesis of microwave heating ceramics and their microwave deicing performance in dense-graded asphalt mixtures. *J. Cleaner Prod.* **2018**, *170*, 486−495.

(2) Ma, Z.; Liu, G. F.; Zhang, H.; Zhang, S.; Lu, Y. G. Evaluation of pyrite cinders from sulfuric acid production as oxygen carrier for chemical looping combustion. *Energy* **2021**, *233*, 121079.

(3) Jiang, T.; Tu, Y. K.; Su, Z. J.; Lu, M. M.; Liu, S.; Liu, J. C.; Gu, F. Q.; Zhang, Y. B. A novel value-added utilization process for pyrite cinder: Selective recovery of Cu/Co and synthesis of iron phosphate. *Hydrometallurgy* **2020**, *193*, 105314.

(4) Jin, W.; Yang, S. H.; Tang, C. B.; Li, Y.; Chang, C.; Chen, Y. M. Green and short smelting process of bismuth sulphide concentrate with pyrite cinder. *J. Cleaner Prod.* **2022**, *377*, 134348.

(5) Sun, J. W.; Han, P. W.; Liu, Q.; Ding, J.; Qian, P.; Ye, S. F. Pilot plant test on the recovery of valuable metals from pyrite cinder by a combined process based on chlorinating roasting. *Trans. Indian Inst. Met.* **2019**, *72*, 1053−1061.

(6) Lv, Y. A.; Chen, D.; Tang, J. G.; Li, J.; Yang, D. R.; Chen, B. X. Recovery of iron from pyrite cinder with reduction-magnetic separation process in presence of sodium salt. *Trans. Indian Inst. Met.* **2019**, *72*, 501−510.

(7) Li, Y.; Xue, H. T.; Taskinen, P.; Yang, S. H.; Tang, C. B.; Jin, W.; Chen, Y. M.; Jokilaakso, A. Sustainable phase-conversion method for antimony extraction and sulfur conservation and waste treatment at low temperature. *J. Cleaner Prod.* **2020**, *268*, 121950.

(8) Bai, S. J.; Bi, Y. X.; Ding, Z.; Li, C. L.; Yu, P.; Wen, S. M. Innovative methodology for the utilization of low-grade pyrite cinder containing heavy metals via hydrothermal alkali melting followed by chlorination roasting. *J. Alloys Compd.* **2020**, *840*, 155722.

(9) Zhang, H. Q.; Chen, G. H.; Cai, X.; Fu, J. T.; Liu, M. X.; Zhang, P. F.; Yu, H. The leaching behavior of copper and iron recovery from reduction roasting pyrite cinder. *J. Hazard. Mater.* **2021**, *420*, 126561.

(10) Wang, Y. L.; Xiao, L.; Liu, H. X.; Qian, P.; Ye, S. F.; Chen, Y. F. Acid leaching pretreatment on two-stage roasting pyrite cinder for gold extraction and co-precipitation of arsenic with iron. *Hydrometallurgy* **2018**, *179*, 192−197.

(11) Liu, L. H.; Dong, W. H.; Niu, M. Y.; Liu, X.; Xue, J. R.; Tang, A. P. Fabrication of a confined pyrite cinder-based photo-Fenton catalyst and its degradation performance for ciprofloxacin. *J. Mol. Liq.* **2022**, *360*, 119489.

(12) Kerkez, D.; Becelic-Tomin, M.; Gvoic, V.; Mandic, A. K.; Macerak, A. L.; Pilipovic, D. T.; Pesic, V. Pyrite cinder as an effective Fenton-like catalyst for the degradation of reactive azo dye: Effects of process parameters and complete effluent characterization. *Catalysts* **2023**, *13*, 424.

(13) Cao, X.; Chen, Y.; Liang, X.; Li, Y.; Zhang, W.; Cai, Z.; Zhang, T. Basic research on selective extraction of iron from titanium dioxide waste acid to prepare iron phosphate precursors. *Separations* **2023**, *10*, 400.

(14) Hao, X.; Lu, L.; Liang, B.; Li, C.; Wu, P.; Wang, J. Solvent extraction of titanium from the simulated ilmenite sulfuric acid leachate by trialkylphosphine oxide. *Hydrometallurgy* **2012**, *113−114*, 185−191.

(15) Zhang, W. G.; Zhang, T. A.; Cai, L. L.; Lv, G. Z.; Cao, X. J. Preparation of doped iron phosphate by selective precipitation of iron from titanium dioxide waste acid. *Metals* **2020**, *10*, 789.

(16) Ju, J. R.; Feng, Y. L.; Li, H. R.; Xu, C. L. Extraction of valuable metals from acidic wastewater and blast furnace slag by a collaborative utilization process. *Asia-Pac. J. Chem. Eng.* **2022**, *17*, No. e2777.

(17) Ju, J. R.; Feng, Y. L.; Li, H. R.; Xu, C. L. Resource utilization of strongly acidic wastewater and red gypsum by a harmless self-treatment process. *Process Saf. Environ. Prot.* **2023**, *172*, 594−603.

(18) Song, Y. W.; Wang, H. R.; Wang, R.; Zhou, J. C. Novel approach for high-efficiency recovery of titanium dioxide, hydrochloric acid, and organic solvents from titanium white waste acid. *J. Cleaner Prod.* **2021**, *315*, 128105.

(19) Ma, G. Q.; Cheng, M. Experimental study on preparation of titanium-rich material by pressure leaching of titanium concentrate from titanium dioxide waste acid. *Ferroelectrics* **2021**, *581*, 281−286.

(20) Nguyen, N. V.; Hai, P. D.; My My, V. T.; Men, D. T.; Trung, L. D.; Bavor, H. J. Improving product added-value from shrimp (*Litopenaeus vannamei*) waste by using enzymatic hydrolysis and response surface methodology. *J. Aquat. Food Prod. Technol.* 2021, 880−892. .

(21) Bai, X.; Wen, S. M.; Liu, J.; Lin, Y. L. Response surface methodology for optimization of copper leaching from refractory flotation tailings. *Minerals* **2018**, *8* (4), 165.

(22) Zhang, Z. Y.; Peng, J. H.; Srinivasakannan, C.; Zhang, Z. B.; Zhang, L. B.; Fernández, Y.; Menéndez, J. A. Leaching zinc from spent catalyst: Process optimization using response surface methodology. *J. Hazard. Mater.* **2010**, *176*, 1113−1117.

(23) Liu, J.; Wen, S. M.; Liu, D.; Lv, M. Y.; Liu, L. J. Response surface methodology for optimization of copper leaching from a low-grade flotation middling. *Miner. Metall. Process.* **2011**, *28* (3), 139−145.

(24) Javed, U.; Farooq, R.; Shehzad, F.; Khan, Z. Optimization of HNO_3 leaching of copper from old AMD Athlon processors using response surface methodology. *J. Environ. Manage.* **2018**, *211*, 22−27.

(25) Ferreira, S. L. C.; Bruns, R. E.; Ferreira, H. S.; Matos, G. D.; David, J. M.; Brandão, G. C.; da Silva, E. G. P.; Portugal, L. A.; dos Reis, P. S.; Souza, A. S.; dos Santos, W. N. L. Box-Behnken design: an alternative for the optimization of analytical methods. *Anal. Chim. Acta* **2007**, *597*, 179−186.

https://doi.org/10.1021/acsomega.3c09815
ACS Omega 2024, 9, 8510−8519